Journal of Cranio-Maxillo-Facial Surgery 54 (2026) 104523

Contents lists available at ScienceDirect

Journal of Cranio-Maxillo-Facial Surgery

journal homepage: www.jcmfs.com

Morphological analysis of posterior fossa in Apert and Crouzon syndromes before and after posterior cranial vault expansion

Ruonan Dong [a], Ce Liang [a], Susan E. Evans [b], David Johnson [c], Wuyang Shui [d], Christian Duncan [d], Roman H. Khonsari [e,f], Giovanna Paternoster [g], Mehran Moazen [a,*]

[a] Department of Mechanical Engineering, University College London, London, WC1E 7JE, UK
[b] Department of Cell and Developmental Biology, University College London, WC1E 6BT, UK
[c] Oxford Craniofacial Unit, Oxford University Hospital, Oxford, OX3 9DU, UK
[d] Department of Craniofacial Surgery, Alder Hey Children's Hospital, Liverpool, L12 2AP, UK
[e] Department of Maxillo-Facial Surgery and Plastic Surgery, Necker – Enfants Malades University Hospital, Assistance Publique – Hôpitaux de Paris, Université de Paris, Paris, 75015, France
[f] Craniofacial Growth and Form Laboratory, Imagine Institute, Paris, France
[g] Department of Neurosurgery, Craniofacial surgery unit, Necker – Enfants Malades University Hospital, Assistance Publique – Hôpitaux de Paris, Université de Paris, Paris, 75015, France

ARTICLE INFO

Keywords:
Craniosynostosis
Skull
Biomechanics
Intracranial volume
Morphometric

ABSTRACT

Background: Syndromic craniosynostosis, such as Apert and Crouzon syndromes, involve premature fusion of cranial sutures, leading to cranial deformities and potential neurological complications. Posterior cranial vault expansion (PCVE) is commonly used to address intracranial volume (ICV) anomalies in these cases, especially in the posterior fossa region. However, the morphological variation of this region between normal, Apert and Crouzon individuals remains understudied. This study aimed to carry out a detailed morphological analysis of the posterior fossa between the aforementioned groups before and after PCVE.

Methods: Retrospective computed tomography (CT) data from 28 children with Apert (n = 13) and Crouzon (n = 15) syndromes, alongside 51 age-matched controls, were analyzed. Intracranial and posterior fossa volumes (ICV and PFV) were computed pre- and post-operatively. Morphometric shape analyses were conducted for posterior fossa and intracranial cavity using principal component analysis (PCA).

Results: Pre-operatively, Apert syndrome patients exhibited larger PFV and ICV compared to Crouzon syndrome patients and controls (e.g., $p = 0.009$ for pre-operative Apert vs. controls), while Crouzon syndrome patients showed more variability in PFV and ICV. Post-operatively, Apert patients demonstrated significant increases in both PFV and PFV/ICV ratios (e.g., post-operative vs. pre-operative PFV: $p < 0.001$). In contrast, Crouzon patients exhibited limited improvements in PFV, with PFV/ICV ratios often declining post-surgery ($p = 0.890$; median post-operative–pre-operative difference = −0.095). PCA revealed distinct intracranial and posterior fossa shape differences between Apert and Crouzon patients.

Conclusions: While PCVE increased posterior fossa volume, it did not appear to improve posterior fossa shape in either Apert or Crouzon patients. Future studies are required to address the limitations of small sample sizes, lack of post-operative data on Chiari anomaly, and surgical variability to further explore possible correlations between the aforementioned parameters.

1. Introduction

Craniosynostosis is a congenital condition involving the premature fusion of one or more cranial sutures. This early fusion restricts growth perpendicular to the fused suture, leading to characteristic cranial deformities due to the compensatory expansion of adjacent unaffected sutures and localized overgrowth parallel to the fused suture, known as Virchow's law (e.g. Persing et al., 1989; Johnson and Wilkie, 2011; Flaherty et al., 2016). Syndromic craniosynostosis is a more severe form of the condition when cranial deformities are exhibited alongside

* Corresponding author.
E-mail address: m.moazen@ucl.ac.uk (M. Moazen).

https://doi.org/10.1016/j.jcms.2026.104523
Received 20 May 2025; Received in revised form 30 January 2026; Accepted 19 February 2026
Available online 25 February 2026

systemic abnormalities with a range of impacts, such as on the respiratory and musculoskeletal systems. Apert and Crouzon syndrome are frequently encountered in large craniofacial practices, associated with mutations in the Fibroblast Growth Factor Receptor 2 (FGFR2) gene and presenting in most cases with bicoronal suture fusion (Johnson and Wilkie, 2011), along with abnormalities in skull base synchondroses, particularly around the foramen magnum (Kreiborg et al., 1993; Coll et al., 2018; Wang et al., 2022).

Apert and Crouzon syndromes cause significant craniofacial deformities, impacting both aesthetic and functional aspects of a child's life. Additionally, the constriction of the posterior fossa may lead to Chiari Malformation, where brain tissue extends beneath the foramen magnum into the spinal canal, potentially causing neurological symptoms (Aydin et al., 2005; Furtado et al., 2009; Dagtekin et al., 2011). Management of syndromic craniosynostosis typically involves a staged surgical approach to address both functional and cosmetic concerns. Posterior cranial vault expansion (PCVE) has become the preferred initial intervention in many centers (Mathijssen, 2015, 2021; Swanson et al., 2016; Wu et al., 2024), aiming to expand the intracranial volume and prevent/release the elevated intracranial pressure (ICP) by gradually separating the bones at the back of the skull. Subsequent procedures, such as fronto-facial advancement and midfacial osteotomies, are performed as the child grows to address evolving craniofacial needs.

A number of studies have described and compared different treatment techniques for PCVE, including the use of distractors (Ong et al., 2014; Thomas et al., 2014; Di Rocco et al., 2018; Al-Shaqsi et al., 2023), springs (Arnaud et al., 2012; Breakey et al., 2021), and the free-floating bone flap (Di Rocco et al., 2012; Tamburrini et al., 2021). Several studies have examined the posterior fossa volume in Apert and Crouzon children and performed linear calvarial measurements (Kanodia et al., 2012; Lu et al., 2019, 2020; Al-Shaqsi et al., 2023). However, to the best of our knowledge, there is a lack of detailed morphological analysis of posterior fossa in Apert and Crouzon patients. The aim of this study was to characterize morphological differences of the intracranial cavity, posterior fossa, and foramen magnum between Apert and Crouzon patients (vs. a control group), and to evaluate their changes following PCVE in a limited number of cases. Understanding these distinctions could inform whether management strategies should differ for Apert and Crouzon children.

2. Materials and methods

2.1. Patient data

Retrospective computed tomography (CT) images were obtained for children diagnosed with Apert and Crouzon syndromes from Necker–Enfants Malades University Hospital, Paris (NE - n = 18), and Alder Hey Children's Hospital, Liverpool (AH - n = 10). The inclusion criteria for these children were: (1) undergone posterior cranial vault expansion as the first surgical intervention (excluding shunt procedures), and (2) availability of CT scans at both pre-operative and post-operative stages for comparative analysis. Additionally, CT scans from a control group (n = 51) were acquired from Necker–Enfants Malades University Hospital (Liang et al., 2024). These were selected from a larger database (n = 217) that was previously described and characterized (Galiay et al., 2022; Liang et al., 2023). ANOVA indicated no significant difference between the two regression models of cranial module by age computed based on the control groups of 51 and 217 individuals (p = 0.5505, Fig. S1). All CT data was anonymized, and data collection and analysis were conducted in accordance with relevant ethical guidelines and regulations.

2.2. Institutional strategy for treatment of Apert and Crouzon patients

At both Necker–Enfants Malades University Hospital and Alder Hey Children's Hospital, the surgical management of syndromic craniosynostosis is conducted within a multidisciplinary framework involving neurosurgeons, craniofacial surgeons, radiologists, and paediatricians. Diagnosis is based on a combination of clinical assessment for raised intracranial pressure (ICP), characteristic craniofacial morphology, ophthalmological findings, and radiological confirmation of suture fusion on computed tomography (CT). In patients with syndromic craniosynostosis, posterior cranial vault expansion (PCVE) is performed as a staged procedure at both centers. PCVE is typically planned between 6 and 12 months of age, with timing and indication determined by the presence of bicoronal or multisuture fusion, associated comorbidities, disease severity, craniofacial morphological features, and radiological findings.

At Necker–Enfants Malades Hospital, several surgical techniques are employed for PCVE; however, there are currently no formal guidelines to support the selection between these methods. Bone thickness is the primary factor guiding the choice between free bone flaps or spring-assisted techniques versus distractor-based expansion, as secure screw fixation is challenging in very young patients with thin calvarial bone. Nevertheless, no quantitative criteria are available to standardize this decision, which largely relies on surgeon experience and clinical judgement. In contrast, at Alder Hey Children's Hospital, distractor-based techniques are systematically selected for PCVE (see also El-Nemr et al., 2025).

Fronto-orbital advancement or monobloc procedures are typically performed at a later stage of craniofacial reconstruction. Following an initial PCVE, patients are closely monitored for the development of obstructive sleep apnoea syndrome (OSAS), raised intracranial pressure (ICP), and ophthalmological complications. Based on the evolving clinical profile, further frontofacial surgery may be indicated. The presence of severe OSAS is the principal criterion guiding the choice between frontofacial advancement (monobloc procedure) and fronto-orbital advancement. The subsequent surgical history of these patients is summarized in the Supplementary Material (Table S1).

2.3. Surgical techniques

Three distinct surgical techniques were employed for the treatment of Apert and Crouzon children included in this study: (1) distractors: following a tailored craniotomy, distractors were applied, with distraction progressing at a rate of 1 mm per day over approximately two weeks to one month. This was followed by a consolidation phase lasting 2–3 months, after which a second procedure was performed to remove the distractors; (2) free-floating bone flap: the flap was left unattached after craniotomy, allowing gradual skull expansion guided by the surrounding soft tissues. Over time, natural bone healing and growth secured the flap in its new position, achieving the desired cranial volume increase; (3) springs: without any craniotomy, translambdoid springs were inserted across the patent lambdoid sutures under tension to exert a gradual outward force, facilitating skull expansion over several weeks. These springs were removed after 3-6 months once sufficient distraction had been achieved. See Fig. 1 for a schematic illustration of these three techniques. The duration of distraction is determined by the degree of correction of brachycephaly, which is assessed clinically. As with other aspects of management, this decision is not guided by predefined quantitative criteria but relies primarily on clinical judgement.

At Necker–Enfants Malades University Hospital, the cases included in this study for Apert children were treated using distractors, springs, and free-floating bone flaps, while Crouzon children underwent procedures involving distractors and free-floating bone flaps. At Alder Hey Children's Hospital, distractors were selectively used for both Apert and Crouzon cases included in this study.

2.4. Image processing and volumetric analysis

CT scans of the head from all patients at both pre- and post-operative stages, as well as from control group, were reconstructed using Avizo

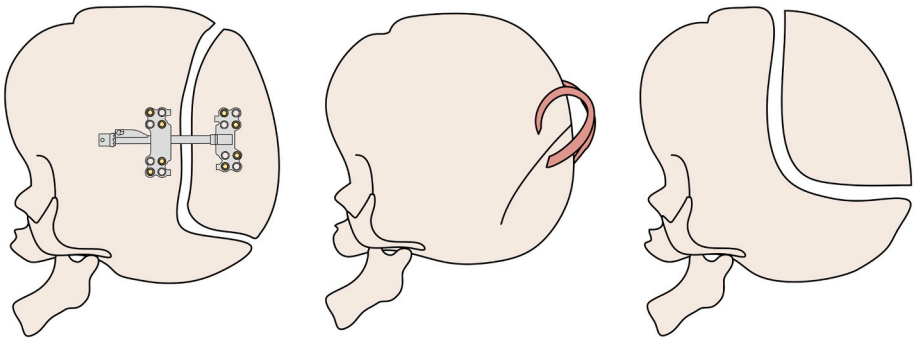

Fig. 1. Illustrations of Posterior Cranial Vault Distraction Methods: distractors (left), springs (middle), and free-floating bone flap method (right).

software (v2022.1, Thermo Fisher Scientific, MA, USA). The surfaces of the intracranial cavity were extracted from the reconstructed skull models, and intracranial volume (ICV) was calculated using an R-based tool, *endomaker* (Profico et al., 2020; Buzi et al., 2023). The surface representing the posterior fossa region was isolated from the previously extracted intracranial cavity surface using Geomagic Wrap software (v2021, Oqton, Ghent, Belgium), based on anatomical landmarks (detailed below), and the posterior fossa volume (PFV) was calculated using the same R-based tool (Fig. 2A).

2.5. Morphometric analysis

Nineteen anatomical landmarks (LM) were identified on each posterior cranial fossa to guide the placement and sliding of another 200 surface semi-landmarks (Fig. 2B), prepared for the linear measurement and further geometric morphometric analysis, following a prior protocol (Liang et al., 2023). The foramen magnum length and width were measured based on relevant LMs, allowing the calculation of the foramen magnum index (the ratio of width by length). An additional pathset was positioned along the boundary of the foramen magnum in Avizo to delineate its margin. The surface area of the foramen magnum was subsequently calculated using the shoelace formula implemented in R

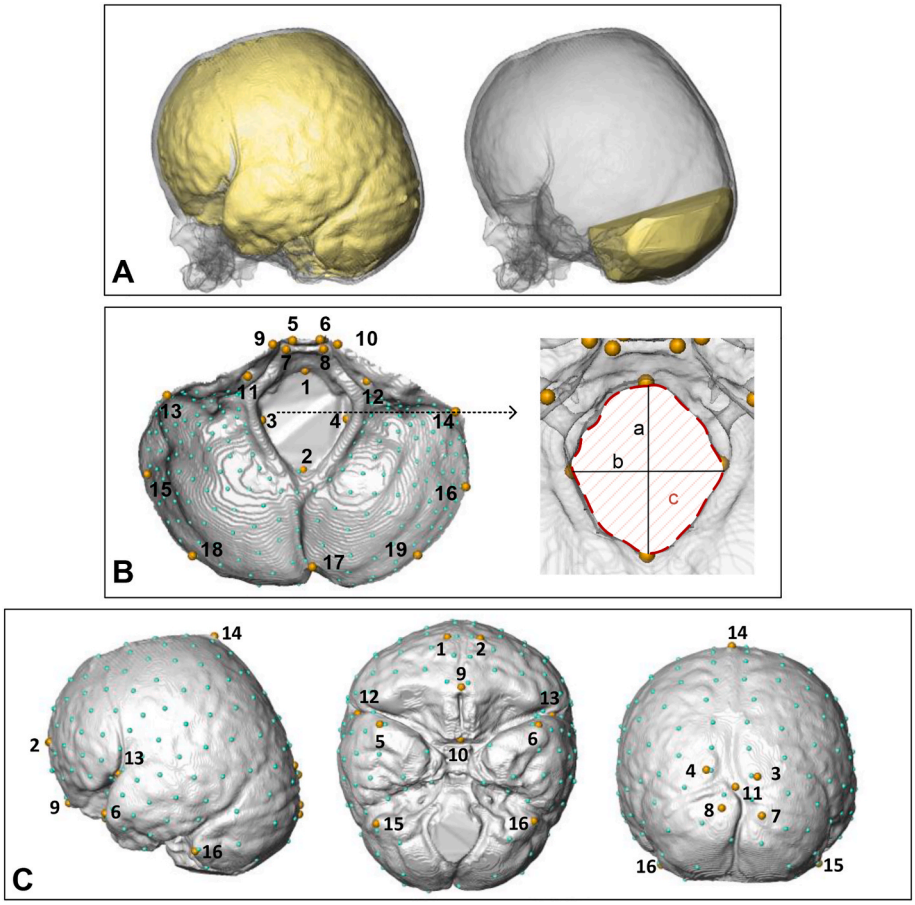

Fig. 2. (A) Reconstructed skull of an Apert syndrome child, showing the endocast (yellow, left) and posterior fossa (yellow, right) overlaid on the skull model (grey). (B) Landmark configurations of the posterior fossa, comprising 19 anatomical landmarks (yellow) and semilandmarks (green). Detailed definitions are provided in Table S2. Two linear dimensions were measured between selected landmarks: foramen magnum length (a) and width (b). The foramen magnum area is outlined by red dashed lines (c). (C) Landmark configurations of the endocast, including 16 anatomical landmarks (yellow) and semilandmarks (green). Detailed definitions are provided in Table S3. (For interpretation of the references to colour in this figure legend, the reader is referred to the Web version of this article.)

(Braden, 1986). Similarly, sixteen LMs were identified on each intracranial cavity surface, and 200 semi-landmarks were placed accordingly (Fig. 2C). Principal component analysis (PCA) of intracranial cavity and posterior fossa shape was performed in R using the *Morpho* package (Profico et al., 2021). To visualize shape variations associated with principal component (PC) vectors, the mean intracranial cavity and posterior fossa shape was warped along each PC vector toward the extremes of the PC scores (Liang et al., 2023).

2.6. Statistical analysis

Statistical analyses were conducted using R (R Core Team, 2024) with the *boot* (Canty and Ripley, 2024; Davison and Hinkley, 1997) and *readr* (Wickham et al., 2024) packages. Numerical variables were summarized using the median and interquartile range (IQR) due to the skewed distribution and small sample size. Categorical variables were summarized as percentages. Wilcoxon rank-sum tests were used for comparisons between independent groups, and Wilcoxon signed-rank tests were used for paired data (e.g. pre- and post-operative measurements). All P values were two-sided, with a $p < 0.05$ considered statistically significant. For each comparison, 95% confidence intervals for median differences were estimated using nonparametric bootstrap resampling with 10,000 iterations.

Table 1
Summary of Apert and Crouzon cases analyzed in this study. Pre- and post-operative values are presented as median (interquartile range, IQR).

		Apert			Crouzon		
Hospital		NE	AH	P value	NE	AH	P value
Demographic data							
Number of cases		8	5	/	10	5	/
	Distractors	4	5	/	6	5	/
	Springs	3	0	/	0	0	/
	Free-floating bone flap	1	0	/	4	0	/
Sex	F	4	4	/	6	3	/
	M	4	1	/	4	2	/
Chiari malformation		0	0	/	5	3	/
Fully fused suture at pre-op	Bicoronal	8	5	/	8	3	/
	Metopic	1	0	/	4	3	/
	Sagittal	1	0	/	3	1	/
	Lambdoid	1	2	/	7	5	/
Pre-operative and post-operative data							
Age (days)	Pre-op	203.0 (172.2–267.0)	162.0 (59.0–204.0)	0.305	256.0 (197.0–369.0)	431.0 (206.0–558.0)	0.440
	Post-op	406.5 (339.5–488.0)	498.0 (424.0–533.0)	0.524	516.0 (380.5–737.2)	855.0 (464.0–937.0)	0.310
	Distractors	447.0 (388.8–488.0)	498.0 (424.0–533.0)	0.556	504.5 (380.5–726.8)	855.0 (464.0–937.0)	0.329
	Springs	395.0 (372.5–528.0)	/	/	/	/	/
	Free-floating bone flap	308.0	/	/	537.0 (399.0–676.5)	/	/
Intracranial volume (mm^3)	Pre-op	1169.9 (1065.1–1259.1)	834.6 (677.5–1005.1)	0.030	982.6 (708.5–1248.1)	1171.1 (905.4–1185.3)	0.440
	Post-op	1400.2 (1364.8–1499.1)	1351.6 (1320.9–1445.9)	0.524	1278.1 (1091.4–1493.0)	1452.0 (1198.1–1454.6)	0.679
	Distractors	1486.7 (1393.8–1630.6)	1351.6 (1320.9–1445.9)	0.191	1452.0 (1147.8–1694.7)	1452.0 (1198.1–1454.6)	0.792
	Springs	1401.6 (1362.2–1437.8)	/	/	/	/	/
	Free-floating bone flap	1187.8	/	/	1165.3 (1040.3–1232.1)	/	/
Posterior fossa volume (mm^3)	Pre-op	110.1 (81.4–127.9)	65.2 (30.8–83.4)	0.045	60.6 (56.5–64.1)	73.8 (72.4–79.4)	0.019
	Post-op	137.0 (126.4–172.5)	112.0 (108.1–118.0)	0.019	81.7 (75.5–86.3)	88.3 (82.4–96.5)	0.207
	Distractors	136.9 (126.4–151.9)	112.0 (108.1–118.0)	0.063	79.1 (75.5–83.7)	88.3 (82.4–96.5)	0.178
	Springs	172.4 (151.0–172.7)	/	/	/	/	/
	Free-floating bone flap	116.0	/	/	84.8 (74.5–87.4)	/	/
FM length (mm)	Pre-op	31.0 (29.7–32.3)	26.5 (23.9–30.9)	0.171	25.3 (23.5–26.0)	26.6 (26.6–28.0)	0.028
	Post-op	32.1 (29.9–34.2)	31.5 (25.0–32.6)	0.622	25.8 (25.1–27.0)	26.2 (26.1–29.4)	0.254
	Distractors	32.1 (29.5–34.3)	31.5 (25.0–32.6)	0.730	26.3 (25.6–29.0)	26.2 (26.1–29.4)	0.537
	Springs	30.1 (30.2–32.1)	/	/	/	/	/
	Free-floating bone flap	34.2	/	/	24.6 (22.6–26.2)	/	/
FM width (mm)	Pre-op	23.1 (22.2–24.8)	20.1 (19.3–21.9)	0.065	18.8 (18.3–21.0)	20.8 (20.1–21.7)	0.165
	Post-op	24.9 (24.2–26.4)	24.9 (22.8–27.0)	0.622	19.9 (19.1–20.8)	22.2 (20.9–22.4)	0.075
	Distractors	24.1 (23.7–25.5)	24.9 (22.8–27.0)	0.905	19.6 (19.1–20.2)	22.2 (20.9–22.4)	0.052
	Springs	25.4 (24.9–27.1)	/	/	/	/	/
	Free-floating bone flap	25.6	/	/	20.4 (19.0–21.5)	/	/
FM area (mm^2)	Pre-op	482.8 (441.3–539.7)	355.6 (350.4–414.8)	0.065	349.0 (302.1–394.6)	389.4 (380.9–417.4)	0.129
	Post-op	555.0 (500.4–595.5)	584.8 (407.9–599.4)	0.833	393.8 (342.9–446.2)	406.5 (403.6–471.5)	0.254
	Distractors	512.6 (477.3–579.7)	584.8 (407.9–599.4)	0.905	393.8 (353.2–442.4)	406.5 (403.6–471.5)	0.247
	Springs	580.2 (543.4–610.7)	/	/	/	/	/
	Free-floating bone flap	566.4	/	/	382.3 (321.5–435.4)	/	/

3. Results

3.1. Patient demographics

A detailed summary of all Apert (n = 13) and Crouzon (n = 15) children included in this study and the aged-matched control (n = 51) children is provided in Table 1. Surgical interventions differed across NE and AH hospitals and considered cases. In the Apert cohort, distractors were predominantly used (NE: n = 4, AH: n = 5), while springs were employed only in NE (n = 3); free-floating bone flaps were minimally utilized, with only 1 case reported in NE. For Crouzon syndrome, distractors were the most common technique in both hospitals (NE: n = 6, AH: n = 5); springs and free-floating bone flaps were not reported for Crouzon cases in either hospital. Chiari malformation was observed in a subset of Crouzon patients (n = 8) across the two hospitals, while it was not reported in any of the Apert cohorts. Most cases (n = 24) in both Apert and Crouzon groups presented with complete bicoronal suture fusion at preoperative evaluation.

3.2. Volumetric change in intracranial cavity and posterior fossa

Table 1 and Fig. 3 summarize intracranial and posterior fossa volumes and their ratios in Apert and Crouzon patients, stratified by treatment center and surgical technique. Table 2 presents these measures for Apert and Crouzon patients, together with control data restricted to the same age ranges as each subgroup, and reports comparisons between groups. Additional comparisons between Apert and Crouzon patients and age-adjusted estimated control values, derived from regression models fitted to the control data, are provided in the Supplementary (Table S4).

Intracranial volume (ICV): Apert pre-operative ICV was significantly larger in NE cases compared to AH cases ($p = 0.030$ – Table 1). Pre-op Apert cases from AH aligned more closely with the control regression line, while Apert cases from NE exhibited larger pre-op ICVs overall. Post-operatively, ICV increased across both Apert and Crouzon groups. Increases were observed across all surgical techniques, with distractors generally associated with higher values in many cases. Notably, the highest post-operative ICV values for both Apert and Crouzon patients were achieved in cases treated with distractors. Apert

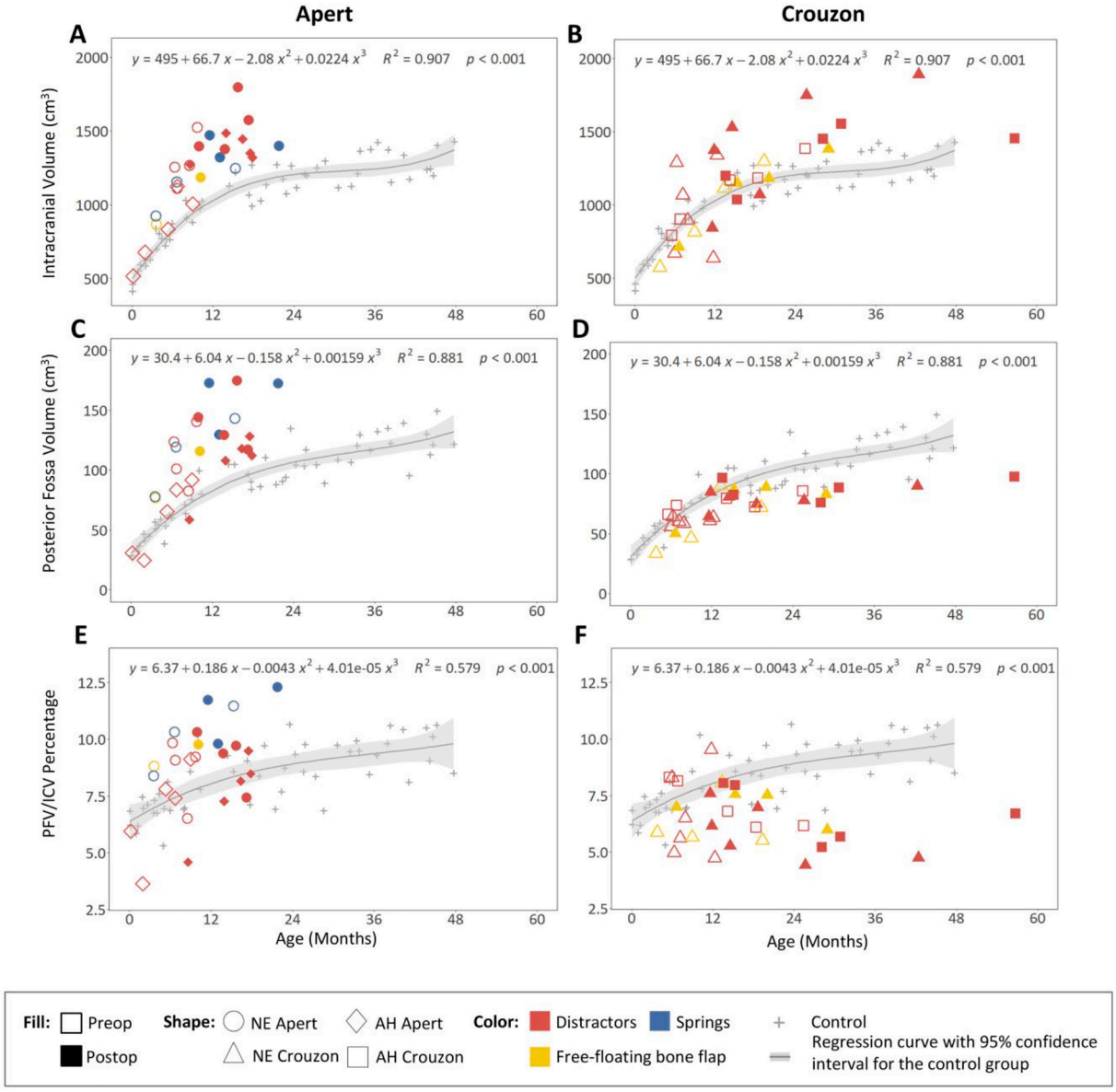

Fig. 3. Intracranial Volume (A, B), Posterior Fossa Volume (C, D), and Posterior Fossa-Intracranial Volume ratio (E,F).

Table 2
Summary of pre- and post-operative Apert and Crouzon cases, together with control data selected within the same age ranges as each subgroup. Values are presented as median (interquartile range, IQR). Group comparisons are reported as p values, median differences, and 95% confidence intervals estimated using bootstrap resampling.

				Number of cases	Age range (days)	Age (days)	Intracranial volume (ICV, mm^3)	Posterior fossa volume (PFV, mm^3)	PFV/ICV percentage (%)	FM index	FM area (mm^2)
pre-op	median (IQR)	A	Apert	13	6 – 466	202 (110–258)	1111.7 (870.2–1247.2)	83.4 (76.7–119.3)	8.8 (7.4–9.2)	0.762 (0.738–0.798)	444.1 (387.0–523.0)
		B	Control of similar ages	22	2 – 465	141 (66–245)	769.8 (624.5–903.5)	55.6 (41.8–69.3)	7.0 (6.8–7.7)	0.751 (0.723–0.814)	439.1 (383.5–561.3)
		C	Crouzon	15	114 – 773	272 (198–418)	1068.5 (805.5–1238.6)	64.3 (59.3–73.1)	6.2 (5.6–8.1)	0.797 (0.739–0.843)	379.4 (326.7–408.5)
		D	Control of similar ages	25	111 – 778	438 (182–604)	1026.6 (873.5–1135.2)	86.1 (62.1–99.4)	8.1 (7.0–8.7)	0.776 (0.731–0.815)	607.5 (494.8–647.5)
	p-value, median difference (95% bootstrap CI)		A vs B - unpaired	/	/	0.357, 60 (-52–136)	0.008, 341.9 (47.8–493.3)	0.009, 27.8 (14.6–66.0)	0.053, 1.85 (0.12–2.33)	0.827, 0.011 (−0.048–0.058)	0.960, 5.0 (−103.3–101.9)
			C vs D - unpaired	/	/	0.394, −166 (-332–127)	0.783, 41.9 (−251.2–265.4)	0.026, −21.8 (−33.0–0.8)	0.003, −1.95 (−2.81–0.36)	0.455, 0.021 (−0.053–0.083)	<0.001, −228.0 (−288.3–-128.8)
			A vs C - unpaired	/	/	0.038, −70 (-263–18)	0.892, 43.2 (−286.9–341.9)	0.019, 19.1 (4.3–57.5)	0.015, 2.64 (0.25–3.45)	0.413, −0.035 (−0.091–0.039)	0.041, 64.6 (−2.4–159.5)
post-op	median (IQR)	E	Apert	13	262 - 661	424 (350–524)	1398.8 (1322.8–1474.0)	128.2 (116.0–144.3)	9.5 (8.2–9.8)	0.841 (0.761–0.856)	566.4 (481.5–599.4)
		F	Control of similar ages	11	272-652	526 (377–560)	1068.1 (1007.9–1177.8)	90.3 (85.0–102.0)	8.6 (8.1–9.2)	0.776 (0.720–0.834)	631.9 (614.5–680.5)
		G	Crouzon	15	201-1725	567 (427–867)	1374.7 (1110.7–1492.0)	82.7 (76.7–88.6)	6.7 (5.5–7.5)	0.800 (0.733–0.852)	406.4 (362.6–457.3)
		H	Control of similar ages	37	182 - 1451	778 (539–1107)	1198.0 (1076.1–1268.4)	104.6 (90.3–121.1)	9.0 (8.4–9.8)	0.776 (0.731–0.815)	650.4 (566.0–719.2)
	p-value, median difference (95% bootstrap CI)		E vs F - unpaired	/	/	0.361, −102 (-189–108)	<0.001, 330.7 (177.5–447.3)	<0.001, 37.9 (16.6–56.3)	0.252, 0.91 (−0.80–1.92)	0.331, 0.065 (−0.043–0.135)	0.009, −65.5 (−169.9–-25.0)
			G vs H - unpaired	/	/	0.237, −211 (-509–160)	0.107, 176.7 (−79.7–325.7)	<0.001, −21.9 (−33.5–-11.1)	<0.001, −2.35 (−3.61–-1.05)	0.447, −0.005 (−0.083–0.056)	<0.001, −244.0 (−309.8–-181.7)
			E vs G - unpaired	/	/	0.080, −143 (-455–60)	0.363, 24.1 (−129.2–315.2)	<0.001, 45.5 (29.1–63.7)	<0.001, 2.78 (0.96–4.13)	0.387, 0.041 (−0.042–0.111)	<0.001, 159.9 (58.0–213.1)
from pre-op to post-op	p-value, median difference (95% bootstrap CI)		E vs A - paired	/	/	<0.001, 214 (195–287)	<0.001, 317.6 (274.4–397.5)	<0.001, 34.5 (29.3–51.9)	0.002, 0.92 (0.49–1.32)	<0.001, 0.048 (0.017–0.055)	<0.001, 57.2 (46.4–119.7)
			G vs C - paired	/	/	<0.001, 252 (193–407)	<0.001, 242.4 (169.0–306.2)	<0.001, 16.3 (8.3–24.5)	0.890, −0.10 (−0.55–0.46)	0.890, −0.001 (−0.037–0.037)	0.022, 27.0 (−3.1–46.8)

patients consistently exhibited larger ICVs compared to controls (pre-operative: $p = 0.008$, median difference = 341.9; post-operative: $p < 0.001$, median difference = 330.7 – Table 2), with a more uniform distribution. In contrast, Crouzon patients displayed more variability, indicating greater dispersion in ICV trends within this group (Fig. 3A and B).

Posterior fossa volume (PFV): Pre-operatively, PFV in Apert patients was generally higher than the control regression line ($p = 0.009$, median difference = 27.8 – Table 2). Similar to that of ICV, Apert patients' PFV at AH aligned more closely with the control regression line. Post-operatively, Apert patients demonstrated significant increases in PFV ($p < 0.001$, median difference = 34.5 - Table 2). These post-operative values exceeded the control regression line ($p < 0.001$, median difference = 37.9 – Table 2), particularly in the NE cohort. Crouzon patients, in contrast, exhibited pre-op PFV values lower than the control regression line in most cases ($p = 0.026$, median difference = −21.8 – Table 2). Post-operatively, PFV increased modestly but remained below the control regression line ($p < 0.001$, median difference = −21.9 – Table 2 and Fig. 3C and D).

PFV/ICV ratio: Pre-operatively, both Apert and Crouzon patients exhibited dispersed PFV/ICV ratios around the control regression line. Apert patients tended to cluster above the control trend ($p = 0.053$, median difference = 1.85 percentage points - Table 2), indicating relatively higher ratios, while Crouzon patients generally distributed closer to or below controls ($p = 0.003$, median difference = −1.95 percentage points – Table 2). Post-operatively, Apert patients showed a marked increase in PFV/ICV ratios ($p = 0.002$, median difference = 0.92 percentage points – Table 2), with many surpassing control levels, suggesting a treatment effect. In contrast, Crouzon patients consistently displayed ratios lower than control, with a noticeable decline post-surgery ($p = 0.890$, median difference = −0.10 percentage points – Table 2), suggesting a worsening trend in the relative growth of PFV compared to ICV (Fig. 3E and F). Furthermore, a Wilcoxon rank-sum test revealed a statistically significant difference ($p < 0.05$) in PFV/ICV ratios between the Chiari and non-Chiari Crouzon subgroups. This comparison plot is provided in Fig. S2.

3.3. Intracranial and posterior fossa shape analysis

Posterior fossa shape: A shape PCA was carried out using the full landmark and semi-landmark configurations for total 107 samples (Fig. 4A). The first two PCs accounted for more than 60% of the total shape variance (PC1 = 43.6% of the sample variance, PC2 = 17.9%). The inset warping models adjacent to the PCA plot illustrate how posterior fossa morphology transitions across minimum to maximum PC1 and PC2 values. The distribution of scores along PC1 indicates significant morphological variability. Positive PC1 scores are associated with a deeper posterior fossa, an elongated internal occipital crest, and a more horizontally aligned and contracted petrous temporal bridge. Additionally, the frontal portion of the posterior fossa near the petrous temporal bridge was also contracted, contributing to the overall compressed appearance in this region. PC2, that explained a smaller proportion of the variance, captured additional shape differences. Positive PC2 scores were associated with a smaller foramen magnum and a slightly deeper and wider occipital part. The extent of the local change differences is shown in Fig. 4B.

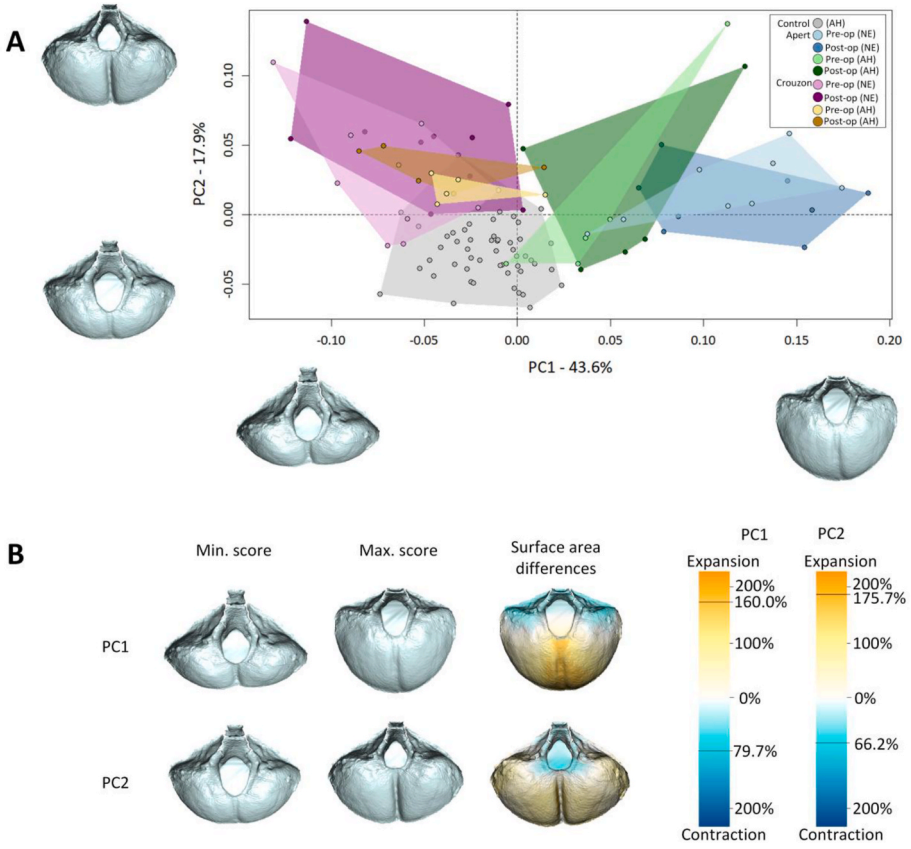

Fig. 4. Principal component analysis (PCA) of full landmark and semi-landmark configurations of Posterior Fossa: shape analysis of control, Apert and Crouzon children pre-op and post-op from NE and AH. (A) The first two PCs (PC1 = 43.6% of total variance, PC2 = 17.9%). (B) Colour maps of surface area changes between the maximum and minimum PC values. Note that the colour map indicates the relative changes in surface area between the minimum surface (reference) and maximum surface (target). Positive percentages represent relative expansion of specific regions from the reference surface to the target surface. The two black lines displayed on scalebar show the limits of surface area expansion or contraction. (For interpretation of the references to colour in this figure legend, the reader is referred to the Web version of this article.)

The control group formed a compact cluster, indicating minimal shape variability. Both Apert and Crouzon groups showed distinct deviations from the control group. The Apert and Crouzon pre-operative groups from AH were positioned closer to the control group, suggesting less severe pre-operative shape deviations compared to their NE counterparts. Apert and Crouzon also display notable differences from each other: Apert clustered along positive PC1, while Crouzon clustered at negative PC1, closer to the control group. Both groups, however, were more evenly distributed along the positive PC2 axis. Post-operatively, only Crouzon from NE showed a minor shift toward the control cluster, while the other post-operative groups appear to move further from the control, indicating minor worsening of the shape. A form (shape and size) PCA plot, which also considers posterior fossa size variability, provides additional context for these shape deviations (Fig. S3).

Intracranial cavity shape: A shape PCA was carried out for the intracranial cavity, with the first two PCs accounting for more than 55% of the total shape variance (PC1 = 31.94% of the sample variance, PC2 = 23.41%). The inset warping models adjacent to the PCA plot illustrate how intracranial morphology transitions from minimum to maximum PC1 and PC2 values (Fig. 5A). Positive PC1 showed an intracranial cavity compressed along the anterior-posterior axis, resulting in a long, flattened posterior region, aligning with the posterior fossa PCA results. Negative PC2 showed a smaller skull base and anterior cranial fossa, that in turn makes the middle cranial fossa appear relatively larger. The extent of these local changes is visualized in Fig. 5B.

The control group again forms a compact cluster, primarily at negative PC1 and positive PC2, indicating minimal shape variability. Apert and Crouzon groups exhibit distinct separation in intracranial cavity shape, with Apert clustering at positive PC1 and Crouzon at negative PC1, closer to the control cluster. Both Apert and Crouzon were evenly distributed along PC2. All groups show pre-operative-to-post-operative shifts. While Crouzon intracranial cavity tend to be closer to the control group post-operatively, Apert endocasts exhibit greater correction overall. Pre-operative AH Crouzon already overlapped with the control cluster, and post-operative results showed minimal differences from control morphology. A form PCA plot which also considers the intracranial cavity size variability is provided in supplementary (Fig. S4).

3.4. Foramen magnum

Table 1 summarises foramen magnum length, width, and area measurements across all cases, stratified by treatment center and surgical technique. Fig. 6 illustrates the foramen magnum index (FMI) and area. Table 2 presents FMI and area values together with control data restricted to the same age ranges as each subgroup and reports comparisons between groups. Additional comparisons between Apert and Crouzon patients and age-adjusted estimated control values, derived from regression models fitted to the control data, are provided in the Supplementary (Table S4). FMI exhibited considerable variability in the control group with an R^2 value of 0.117, indicating a weak correlation with age. Apert children generally clustered closer to the control regression line preoperatively, while Crouzon children showed a broader scatter in FMI values. Post-operatively, FMI showed a

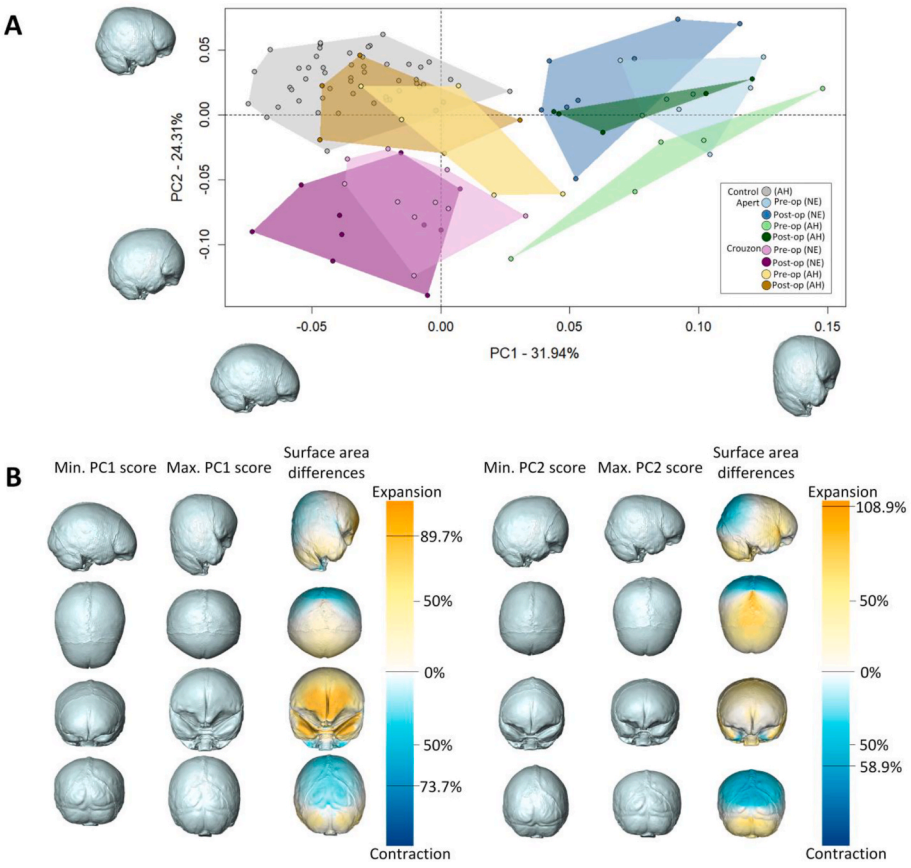

Fig. 5. Principal component analysis (PCA) of full landmark and semi-landmark configurations of intracranial cavity: shape analysis of control, Apert and Crouzon children pre-op and post-op from NE and AH. (A) The first two PCs (PC1 = 31.94% of total variance, PC2 = 24.31%). (B) Colour maps of surface area changes between the maximum and minimum PC values. Note that the colour map indicates the relative changes in surface area between the minimum surface (reference) and maximum surface (target). Positive percentages represent relative expansion of specific regions from the reference surface to the target surface. The two black lines displayed on scalebar show the limits of surface area expansion or contraction. (For interpretation of the references to colour in this figure legend, the reader is referred to the Web version of this article.)

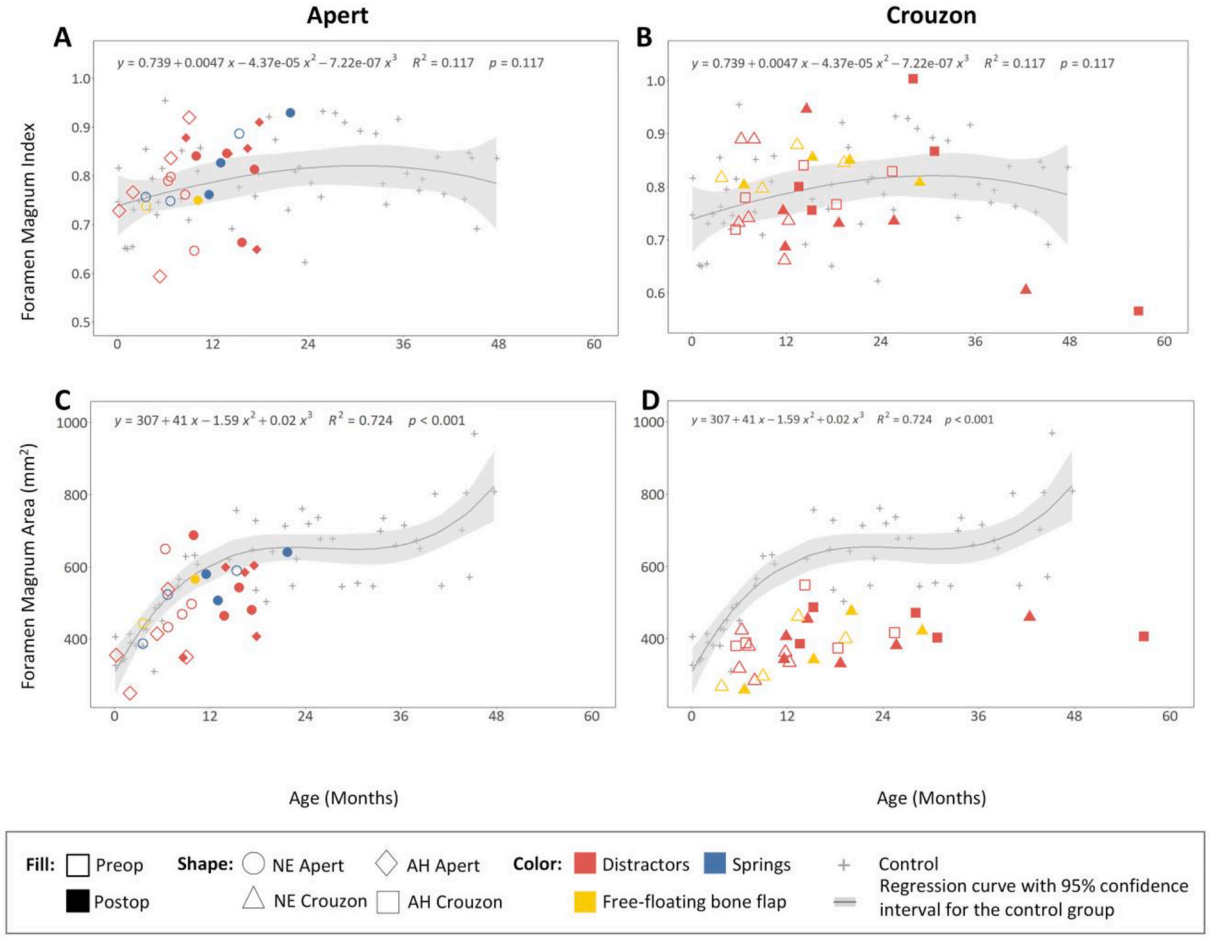

Fig. 6. Foramen magnum index (A, B) and area (C, D).

statistically significant but modest increase in Apert patients ($p < 0.001$, median difference = 0.048 – Table 2), whereas no significant change was observed in Crouzon patients ($p = 0.890$, median difference = −0.001 – Table 2). Despite this, FMI values in both groups remained variable, with no clear overall trend apparent; the Crouzon group additionally exhibited two notable outliers at older ages. The foramen magnum area (FMA) showed a stronger correlation with age, as indicated by an R^2 value of 0.724 for the control data (Fig. 6). Preoperatively, Apert patients had FMA values closer to the control regression line ($p = 0.960$, median difference = 5.0 – Table 2) and higher than those of Crouzon patients ($p = 0.041$, median difference = 64.6 – Table 2). Post-operatively, Apert patients demonstrated a statistically significant increase in FMA ($p < 0.001$, median difference = 57.2 – Table 2), with values approaching but remaining below control levels ($p = 0.009$, median difference = −65.5 – Table 2). In contrast, Crouzon patients exhibited a statistically significant but modest post-operative increase in FMA ($p = 0.022$, median difference = 27.0 – Table 2), with values generally remaining below control levels ($p < 0.001$, median difference = −244.0 – Table 2).

4. Discussion

An increase in intracranial volume (ICV) is considered to be a critical goal of craniosynostosis surgery, as it contributes to reduce the risk of complications such as elevated ICP. The significant post-operative increases in ICV observed in both Apert and Crouzon patients in this study reinforce the effectiveness of posterior cranial vault expansion in achieving volumetric expansion. However, notable differences in volumetric and morphological changes following PCVE between these two syndromes underscore the importance of tailored surgical planning.

Apert patients typically present with normal or even enlarged ICV and posterior fossa volume (PFV) compared to controls, even preoperatively (Gosain et al., 1995; Sgouros et al., 1999; Breakey et al., 2018; Lu et al., 2020), a finding consistent with our study. While PCVE still achieve additional volumetric expansion, the primary challenge appears to be the correction of cranial shape rather than mere intracranial enlargement. In this study, PCA analysis revealed that while PCVE contributed modestly to overall cranial morphology in Apert patients, with post-operative intracranial cavity shapes shifting closer to controls, it had limited or no effect on posterior fossa shape abnormalities. The enlargement of ICV and PFV without sufficient shape normalization highlights a limitation of PCVE as a standalone approach for addressing the complex cranial deformities in Apert syndrome. While PCVE seems essential for alleviating elevated ICP—a key indication for early intervention (Marucci et al., 2008)—these results suggest that alternative or adjunctive surgical strategies may be necessary to achieve comprehensive morphological correction, particularly for the posterior fossa.

The Crouzon cohort demonstrates a different response with persistently low PFV, even after PCVE, aligning with previous studies (e.g. Lu et al., 2019; Pellerin et al., 2021). This limited expansion may be attributed to premature synostosis of the lambdoid suture – as most Crouzon children in this study lacked patent lambdoid sutures at the time of surgery (Table 1), fusion of synchondrosis on the skull base (e.g. Hoshino et al., 2023), or low fibrous attachments of the tentorium. Consequently, current PCVE osteotomies primarily increase volume superior to the tentorium, resulting in disproportionately large intracranial volume expansion relative to a modest PFV increase. Although

PFV does increase post-operatively, this disproportion highlights a crucial limitation in existing surgical strategies. These findings emphasize the necessity for meticulous surgical planning, potentially involving lower osteotomies or placement of distractors closer to the skull base. These anatomical constraints likely limit the effectiveness of PCVE in addressing both intracranial and posterior fossa volume deficiencies in Crouzon cohort. Similar to the Apert children, while the intracranial cavity shape in Crouzon children showed minor improvements post-operatively, the posterior fossa shape demonstrated no improvement. However, despite having lower PFV and ICV compared to Apert children, both intracranial cavity and posterior fossa shape in Crouzon children appeared closer to normal. This discrepancy between volume and shape suggests that while volume expansion is critical, posterior fossa morphology in Crouzon patients may inherently deviate less from the norm than in Apert patients.

Abnormally small bony posterior fossa are often described as being responsible for Chiari Malformation (Aydin et al., 2005; Dagtekin et al., 2011; Furtado et al., 2009; Tubbs et al., 2003). The high prevalence of Chiari malformation in Crouzon children in this study, despite their relatively more normal intracranial cavity and posterior fossa shape compared to Apert patients, suggests that posterior fossa volume (PFV), rather than shape, plays a more critical role in Chiari development. While a previous study by Rijken et al. (2015) suggested that PFV volume and PFV/ICV ratio are not reliable predictors of Chiari malformation in craniosynostosis patients (measured on MRI images), our findings challenge this assertion. We observed a significant difference in PFV/ICV ratios between Chiari and non-Chiari Crouzon subgroups ($p < 0.05$), suggesting that PFV/ICV may hold predictive value within specific patient subgroups. This discrepancy between two studies may be attributed to differences in study design, patient populations, and/or analytical approaches.

Furthermore, foramen magnum (FM) measurements highlighted a smaller FM area for the Crouzon patients in comparison to both Apert and control. This was in line with study by Assadsangabi et al. (2015). This data together with the fact the ICV of Crouzon patients seems to be very similar to those of control data and also possible fusion of synchondroses in these patients may all explain the higher incidence of Chiari development in Crouzon patients.

Taken together these results reinforce a broader concept of “compartmental” cranial decompression. In Apert syndrome where volumes are large, yet morphological deformities persist, surgical strategies might emphasize shape correction in addition to volume adjustments. In Crouzon syndrome, where the posterior fossa is inherently smaller, expansion techniques should be carefully tailored to expand the posterior fossa more aggressively, avoiding a disproportionate increase in the supratentorial space alone. These insights underscore the need for refined osteotomy planning and execution, particularly when addressing the challenges of small posterior fossa. By viewing the intracranial contents as discrete compartments, surgeons can adopt more comprehensive decompression strategies to optimize both functional (ICP-related) and morphological outcomes across syndromic craniosynostosis.

This study has several limitations that should be acknowledged. First, the sample sizes for different surgical techniques, particularly springs, were limited, which prevented comparisons across surgical methods and/or meaningful analysis of outcomes between the two hospitals. Hence we refrained from commenting on these data at this point, awaiting larger dataset. Clearly, the overall sample size of cases included in this study are low and more work is required to increase the sample size of such studies. The current analysis is based on data collected from two craniofacial centers. Inclusion of data from other centers would highlight the multicenter variations and substantially strengthen the generalisability and impact of the findings. Second, due to the absence of post-operative MRI data and detailed timelines for Chiari malformation development, the study could not determine when Chiari malformation occurred. Consequently, the Chiari and non-Chiari groups included both pre- and post-PCVD data, limiting the ability to explore the relationship between Chiari development and surgical interventions. Third, skull base synchondroses were not recorded for each case, which constrained a deeper analysis of foramen magnum dimensions and their role in Chiari malformation. Future studies addressing these limitations could provide more robust insights into the relationship between craniosynostosis, Chiari malformation, and surgical outcomes.

Authors’ contributions

R.D.: data curation, formal analysis, funding acquisition, investigation, methodology, validation, visualization, writing—original draft; C. L.: data curation, formal analysis, investigation, methodology, software, validation, visualization; S.E.E.: formal analysis, investigation, validation, supervision; D.J.: conceptualization, funding acquisition, investigation, supervision; W.Y.S.: data curation, validation, visualization; C. D., R.H.K. & G.P.: conceptualization, data curation, funding acquisition, investigation, methodology, resources, supervision, validation; M.M.: conceptualization, formal analysis, funding acquisition, investigation, methodology, project administration, resources, software, supervision, validation, visualization.

All authors contributed to reviewing and editing the manuscript.

Ethics

Ethical approval was obtained for this study from Necker–Enfants Malades University Hospital under protocols No2018RK18 and from Alder Hey Children's Hospital under No7181.

Declaration of AI use

We have not used AI-assisted technologies in creating this article.

Funding

This work was supported by Engineering and Physical Science Research Council (UK) Grant (EP/W008092/1) award to M.M. and Rosetrees Trust, Stoneygate Trust (PGS22/100040) awarded to M.M. and R.D.

Conflict of interest declaration

The authors declare no conflict of interest.

Acknowledgments

The authors thank Antonio Profico and Costantino Buzi for their support throughout this study.

Appendix A. Supplementary data

Supplementary data to this article can be found online at https://doi.org/10.1016/j.jcms.2026.104523.

References

Al-Shaqsi, S., Ching, J.A., Novak, C.B., Forrest, C.R., 2023. Morphometric analysis and outcomes following posterior cranial vault distraction in syndromic and multisuture craniosynostosis. J. Plast. Reconstr. Aesthetic Surg. 87, 379–386. https://doi.org/10.1016/j.bjps.2023.10.101.

Arnaud, E., Marchac, A., Jeblaoui, Y., Renier, D., Di Rocco, F., 2012. Spring-assisted posterior skull expansion without osteotomies. Childs Nerv. Syst. 28, 1545–1549. https://doi.org/10.1007/s00381-012-1843-4.

Assadsangabi, R., Hajmomenian, M., Bilaniuk, L.T., Vossough, A., 2015. Morphology of the foramen magnum in syndromic and non-syndromic brachycephaly. Childs Nerv. Syst. 31, 735–741. https://doi.org/10.1007/s00381-015-2639-0.

Aydin, S., Hanimoglu, H., Tanriverdi, T., Yentur, E., Kaynar, M.Y., 2005. Chiari type I malformations in adults: a morphometric analysis of the posterior cranial fossa. Surg. Neurol. 64, 237–241. https://doi.org/10.1016/j.surneu.2005.02.021.

Braden, B., 1986. The surveyor's area formula. Coll. Math. J. 17, 326–337. https://doi.org/10.1080/07468342.1986.11972974.

Breakey, R.W.F., Knoops, P.G.M., Borghi, A., Rodriguez-Florez, N., O'Hara, J., James, G., Dunaway, D.J., Schievano, S., Jeelani, N.U.O., 2018. Intracranial volume and head circumference in children with unoperated syndromic craniosynostosis. Plast. Reconstr. Surg. 142, 708e–717e. https://doi.org/10.1097/PRS.0000000000004843.

Breakey, R.W.F., van de Lande, L.S., Sidpra, J., Knoops, P.M., Borghi, A., O'Hara, J., Ong, J., James, G., Hayward, R., Schievano, S., Dunaway, D.J., Jeelani, N. ul O., 2021. Spring-assisted posterior vault expansion—a single-centre experience of 200 cases. Childs Nerv. Syst. 37, 3189–3197. https://doi.org/10.1007/s00381-021-05330-5.

Buzi, C., Profico, A., Liang, C., Khonsari, R.H., O'Higgins, P., Moazen, M., Harvati, K., 2023. Icex: advances in the automatic extraction and volume calculation of cranial cavities. J. Anat. 242, 1172–1183. https://doi.org/10.1111/joa.13843.

Canty, A., Ripley, B., 2024. boot: Bootstrap R (S-Plus) Functions. R package version 1.3-31. Available from: https://CRAN.R-project.org/package=boot.

Coll, G., Sakka, L., Botella, C., Pham-Dang, N., Collet, C., Zerah, M., Arnaud, E., Di Rocco, F., 2018. Pattern of closure of skull base synchondroses in crouzon syndrome. World Neurosurg. 109, e460–e467. https://doi.org/10.1016/j.wneu.2017.09.208.

Dagtekin, A., Avci, E., Kara, E., Uzmansel, D., Dagtekin, O., Koseoglu, A., Talas, D., Bagdatoglu, C., 2011. Posterior cranial fossa morphometry in symptomatic adult chiari I malformation patients: comparative clinical and anatomical study. Clin. Neurol. Neurosurg. 113, 399–403. https://doi.org/10.1016/j.clineuro.2010.12.020.

Davison, A.C., Hinkley, D.V., 1997. Bootstrap Methods and Their Applications. Cambridge University Press, Cambridge.

Di Rocco, F., Marchac, A., Duracher, C., Perié, A.C., Vergnaud, E., Renier, D., Arnaud, E., 2012. Posterior remodeling flap for posterior plagiocephaly. Childs Nerv. Syst. 28, 1395–1397. https://doi.org/10.1007/s00381-012-1842-5.

Di Rocco, F., Usami, K., Protzenko, T., Collet, C., Giraudat, K., Arnaud, E., 2018. Results and limits of posterior cranial vault expansion by osteotomy and internal distractors. Surg. Neurol. Int. 9, 217. https://doi.org/10.4103/sni.sni_465_17.

El-Nemr, M., Richardson, D., Duncan, C., England, J., Russell, L., Parks, C., Sinha, A., Ellenbogen, J., Vakharia, V., Hennedige, A.A., 2025. Posterior vault distraction osteogenesis for craniosynostosis—surgical outcomes over 12 years. J. Craniofac. Surg. 36, 491. https://doi.org/10.1097/SCS.0000000000010952.

Flaherty, K., Singh, N., Richtsmeier, J.T., 2016. Understanding craniosynostosis as a growth disorder. Wiley Interdiscip. Rev. Dev. Biol. 5, 429. https://doi.org/10.1002/wdev.227.

Furtado, S.V., Reddy, K., Hegde, A.S., 2009. Posterior fossa morphometry in symptomatic pediatric and adult chiari I malformation. J. Clin. Neurosci. 16, 1449–1454. https://doi.org/10.1016/j.jocn.2009.04.005.

Galiay, L., Hennocq, Q., Cross, C., Arnaud, E., Larysz, D., Kölby, L., Paternoster, G., Khonsari, R.H., Moazen, M., 2022. Management of sagittal craniosynostosis: morphological comparison of eight surgical techniques. Br. J. Oral Maxillofac. Surg. 60, 499–506. https://doi.org/10.1016/j.bjoms.2021.09.017.

Gosain, A.K., McCarthy, J.G., Glatt, P., Staffenberg, D., Hoffmann, R.G., 1995. A study of intracranial volume in Apert syndrome. Plast. Reconstr. Surg. 95, 284–295. https://doi.org/10.1097/00006534-199502000-00008.

Hoshino, Y., Takechi, M., Moazen, M., Steacy, M., Koyabu, D., Furutera, T., Ninomiya, Y., Nuri, T., Pauws, E., Iseki, S., 2023. Synchondrosis fusion contributes to the progression of postnatal craniofacial dysmorphology in syndromic craniosynostosis. J. Anat. 242, 387–401. https://doi.org/10.1111/joa.13790.

Johnson, D., Wilkie, A.O.M., 2011. Craniosynostosis. Eur. J. Hum. Genet. 19, 369–376. https://doi.org/10.1038/ejhg.2010.235.

Kanodia, G., Parihar, V., Yadav, Y.R., Bhatele, P.R., Sharma, D., 2012. Morphometric analysis of posterior fossa and foramen magnum. J. Neurosci. Rural Pract. 3, 261–266. https://doi.org/10.4103/0976-3147.102602.

Kreiborg, S., Marsh, J.L., Michael Cohen, M., Liversage, M., Pedersen, H., Skovby, F., Børgesen, S.E., Vannier, M.W., 1993. Comparative three-dimensional analysis of CT-scans of the calvaria and cranial base in apert and crouzon syndromes. J. Craniomaxillofac. Surg. 21, 181–188. https://doi.org/10.1016/S1010-5182(05)80478-0.

Liang, C., Landi, F., Çetin, I.E., Profico, A., Buzi, C., Dutel, H., Khonsari, R.H., O'Higgins, P., Moazen, M., 2024. Functional adaptation of the infant craniofacial system to mechanical loadings arising from masticatory forces. Proc. R. Soc. B: Biol. Sci. 291, 20240654. https://doi.org/10.1098/rspb.2024.0654.

Liang, C., Profico, A., Buzi, C., Khonsari, R.H., Johnson, D., O'Higgins, P., Moazen, M., 2023. Normal human craniofacial growth and development from 0 to 4 years. Sci. Rep. 13, 9641. https://doi.org/10.1038/s41598-023-36646-8.

Lu, X., Forte, A.J., Steinbacher, D.M., Alperovich, M., Alonso, N., Persing, J.A., 2019. Enlarged anterior cranial fossa and restricted posterior cranial fossa, the disproportionate growth of basicranium in Crouzon syndrome. J. Craniomaxillofac. Surg. 47, 1426–1435. https://doi.org/10.1016/j.jcms.2019.06.003.

Lu, X., Forte, A.J., Wilson, A., Steinbacher, D.M., Alperovich, M., Alonso, N., Persing, J. A., 2020. Cranial fossa volume and morphology development in apert… : plastic and reconstructive surgery. Plast. Reconstr. Surg. 145, 790e–802e. https://doi.org/10.1097/PRS.0000000000006679.

Marucci, D.D., Dunaway, D.J., Jones, B.M., Hayward, R.D., 2008. Raised intracranial pressure in Apert syndrome. Plast. Reconstr. Surg. 122, 1162. https://doi.org/10.1097/PRS.0b013e31818458f0.

Mathijssen, I.M.J., 2021. Updated guideline on treatment and management of craniosynostosis. J. Craniofac. Surg. 32, 371. https://doi.org/10.1097/SCS.0000000000007035.

Mathijssen, I.M.J., 2015. Guideline for care of patients with the diagnoses of craniosynostosis: working group on craniosynostosis. J. Craniofac. Surg. 26, 1735. https://doi.org/10.1097/SCS.0000000000002016.

Ong, J., Iii, R.J.H., Kelley, P., George, T., 2014. Posterior cranial vault distraction osteogenesis: evolution of technique. Semin. Plast. Surg. 28, 163–178. https://doi.org/10.1055/s-0034-1390169.

Persing, J.A., Jane, J.A., Shaffrey, M., 1989. Virchow and the pathogenesis of craniosynostosis: a translation of his original work. Plast. Reconstr. Surg. 83, 738. https://doi.org/10.1097/00006534-198904000-00025.

Profico, A., Buzi, C., Castiglione, S., Melchionna, M., Piras, P., Veneziano, A., Raia, P., 2021. Arothron: an R package for geometric morphometric methods and virtual anthropology applications. Am. J. Phys. Anthropol. 176, 144–151. https://doi.org/10.1002/ajpa.24340.

Profico, A., Buzi, C., Melchionna, M., Veneziano, A., Raia, P., 2020. Endomaker, a new algorithm for fully automatic extraction of cranial endocasts and the calculation of their volumes. Am. J. Phys. Anthropol. 172, 511–515. https://doi.org/10.1002/ajpa.24043.

Rijken, B.F.M., Lequin, M.H., van der Lijn, F., van Veelen-Vincent, M.-L.C., de Rooi, J., Hoogendam, Y.Y., Niessen, W.J., Mathijssen, I.M.J., 2015. The role of the posterior fossa in developing Chiari I malformation in children with craniosynostosis syndromes. J. Craniomaxillofac. Surg. 43, 813–819. https://doi.org/10.1016/j.jcms.2015.04.001.

Sgouros, S., Hockley, A.D., Goldin, J.H., Wake, M.J.C., Natarajan, K., 1999. Intracranial volume change in craniosynostosis. J. Neurosurg. https://doi.org/10.3171/jns.1999.91.4.0617.

Swanson, J.W., Samra, F., Bauder, A., Mitchell, B.T., Taylor, J.A., Bartlett, S.P., 2016. An algorithm for managing syndromic craniosynostosis using Posterior Vault Distraction Osteogenesis. Plast. Reconstr. Surg. https://doi.org/10.1097/PRS.0000000000002127.

Tamburrini, G., Offi, M., Massimi, L., Frassanito, P., Bianchi, F., 2021. Posterior vault "free-floating" bone flap: indications, technique, advantages, and drawbacks. Childs Nerv. Syst. 37, 3143. https://doi.org/10.1007/s00381-021-05281-x.

Thomas, G.P.L., Wall, S.A., Jayamohan, J., Magdum, S.A., Richards, P.G., Wiberg, A., Johnson, D., 2014. Lessons learned in posterior cranial vault distraction. J. Craniofac. Surg. 25, 1721. https://doi.org/10.1097/SCS.0000000000000995.

Tubbs, R.S., Wellons, J.C., Blount, J.P., Grabb, P.A., Oakes, W.J., 2003. Inclination of the odontoid process in the pediatric chiari I malformation. J. Neurosurg. https://doi.org/10.3171/spi.2003.98.1.0043.

Wang, M.M., Haveles, C.S., Zukotynski, B.K., Reid, R.R., Lee, J.C., 2022. The 27 facial sutures: timing and clinical consequences of closure. Plast. Reconstr. Surg. 149, 701. https://doi.org/10.1097/PRS.0000000000008816.

Wickham, H., Hester, J., Bryan, J., 2024. readr: Read Rectangular Text Data. R package version 2.1.5. Available from: https://CRAN.R-project.org/package=readr.

Wu, M., Barnett, S.L., Massenburg, B.B., Ng, J.J., Romeo, D.J., Taylor, J.A., Bartlett, S.P., Swanson, J.W., 2024. Early posterior vault distraction osteogenesis changes the syndromic craniosynostosis treatment paradigm: long-term outcomes of a 23-year cohort study. Childs Nerv. Syst. 40, 2811–2823. https://doi.org/10.1007/s00381-024-06465-x.